

Hybrid Architectures with Few-Bit ADC Receivers: Achievable Rates and Energy-Rate Tradeoffs

Jianhua Mo, Ahmed Alkhateeb, Shadi Abu-Surra, and Robert W. Heath Jr.

Abstract

Hybrid analog/digital architectures and receivers with low-resolution analog-to-digital converters (ADCs) are two low power solutions for wireless systems with large antenna arrays, such as millimeter wave and massive MIMO systems. Most prior work represents two extreme cases in which either a small number of RF chains with full-resolution ADCs, or low resolution ADC with a number of RF chains equal to the number of antennas is assumed. In this paper, a generalized hybrid architecture with a small number of RF chains and finite number of ADC bits is proposed. For this architecture, achievable rates with channel inversion and SVD based transmission methods are derived. Results show that the achievable rate is comparable to that obtained by full-precision ADC receivers at low and medium SNRs. A trade-off between the achievable rate and power consumption for different numbers of bits and RF chains is devised. This enables us to draw some conclusions on the number of ADC bits needed to maximize the system energy efficiency. Numerical simulations show that coarse ADC quantization is optimal under various system configurations. This means that hybrid combining with coarse quantization achieves better energy-rate trade-off compared to both hybrid combining with full-resolutions ADCs and 1-bit ADC combining.

Jianhua Mo, Ahmed Alkhateeb, and Robert W. Heath Jr. are with The University of Texas at Austin (Email: jhmo, aalkhateeb, rheath@utexas.edu). Shadi Abu-Surra was with Samsung Research America-Dallas, Email: {shadi.as}@samsung.com.

This work was done in part when the first author interned with Samsung Research America-Dallas. The authors at the University of Texas at Austin are supported in part by the National Science Foundation under Grant No. NSF-CCF-1319556 and No. NSF-CCF-1527079.

The material in this paper was presented in part at the 20th International ITG Workshop on Smart Antennas in Munich, Germany, March 2016 [1].

I. INTRODUCTION

Massive multiple-input multiple-output (MIMO) is a key feature of next-generation wireless systems. At low-frequencies, massive MIMO supports many users simultaneously and achieves large sum-rates with relatively simple multi-user processing [2]–[4]. At mmWave frequencies, the large antenna arrays, deployed at both the base station and mobile users, guarantee sufficient received signal power [5]–[10]. This allows signal transmission with ultra high data rates thanks to large bandwidths available at the mmWave frequency band [3], [6], [11]. Unfortunately, the high hardware cost and power consumption of mixed-signal components makes a fully-digital transmission solution, that allocates an RF chain per antenna, difficult to realize in practice [12], [13]. To overcome this challenge, new architectures that relax the requirement of associating an RF chain per antenna are being developed [14]. Hybrid analog/digital architectures [15], [16], and 1-bit ADC receivers [17] are two potential solutions. Those two solutions, though, represent two extreme cases in terms of the number of bits and RF chains. In this paper, we explore a generalization of these two architectures, where finite resolution ADCs are used with hybrid combining.

A. *Related work*

Hybrid analog/digital architectures divide the precoding/combining processing between analog and digital domains. They have been proposed for both mmWave and low-frequency massive MIMO systems [15], [18]–[26]. Hybrid architectures employ many fewer radio frequency (RF) chains than the number of antennas, relying on RF beamforming that is normally implemented using networks of phase shifters [15], [18], [19]. Hybrid precoding for diversity and multiplexing gain was investigated in [18], and for interference management in [19], considering general MIMO systems. These solutions, however, did not make use of the special large MIMO characteristics in the design. For mmWave massive MIMO systems, the sparse nature of the channels was exploited to design low-complexity hybrid precoding algorithms [15], assuming perfect channel knowledge at the transmitter. Extensions to the case when only partial channel knowledge is required was considered in [20], [21]. Hybrid precoding algorithms that do not rely on channel sparsity were proposed in [22], [23], with the aim of maximizing the system spectral efficiency. Hybrid precoding was also shown to achieve performance near that of the fully-digital solutions in low-frequency massive MIMO systems when the number of RF chains

is large enough compared to the number of users [24]–[26]. A common limitation of the hybrid architectures adopted in [15], [18], [20]–[27] is the assumption that the receive RF chains include high-resolution analog-to-digital converters (ADCs), which consume high power, especially at mmWave [12]. Another limitation is the extra power consumption of the analog phase shifters, which can have high impact on the energy efficiency of the hybrid combiner. Compared to the conventional fully-digital receiver, the power saved by reducing the number of RF chains in hybrid receiver may be offset by the additional power consumed by the phase shifters.

An alternative to high resolution ADCs is to live with ultra low resolution ADCs (1-4 bits), which reduces power since ADC power grows exponentially with resolution [28], [29]. In [17], [30]–[38], receiver architectures where the received signal at each antenna is directly quantized by low resolution ADCs without any analog combining is considered. At present, the exact capacity of quantized MIMO channel is unknown, except for special cases like the multiple-input single-output (MISO) and single-input multiple-output (SIMO) channels in the low or high SNR regime [17], [30], [39]. Transmitting independent QAM signals [30] or Gaussian signals [32], [35], [36] from each antenna nearly achieves the capacity at low SNR, but is not optimal at high SNR. The case with CSIT was studied in our previous work [17], [40] where two methods were proposed to design the input constellation and precoder to maximize the channel capacity. It was shown that the proposed methods achieve much larger rate than QAM signaling, especially at high SNR. There is also interest in using 1-bit ADCs for the massive MIMO receiver where a large number of ADCs are needed [37], [38], [41], [42]. The achievable rate of the multiuser uplink massive MIMO channel with 1-bit ADCs was analyzed in [38], [42]. Symbol detection algorithms in a similar setup were proposed in [37], [41]. The architecture in [17], [30]–[37], [39]–[44], though, assume that the number of RF chains is equal to the number of antennas, which means that the hardware cost may be high, and no gain is made from possible beamforming processing in the RF domain.

B. Contribution

In this paper, we propose a generalized hybrid architecture with few-bit ADC receivers and draw important conclusions about its energy-rate trade-off. The hybrid architecture and 1-bit ADC receiver architecture studied in the past represent two extreme points in terms of the number of ADC bits and RF chains. In prior work, the hybrid architecture employs a small

number of RF chains but with high resolution ADCs, while the 1-bit ADC receivers assume that the number of RF chains equals the number of antennas. The contributions of this paper are summarized as follows.

- For the transceiver architecture with hybrid precoding/combining and low resolution ADCs, we propose two transmission methods and derive their achievable rates in closed forms. For the channel inversion based method, the inter-stream interference is canceled before quantization and hence the channel can be separated into several parallel SISO channels. For the SVD based method, the additive quantization noise model is used to derive a lower bound of the achievable rate by assuming Gaussian input distribution. We also derive an upper bound of the channel capacity for one-bit quantization. The bound is achieved by the proposed two transmission methods under certain conditions. In simulations, we show that the proposed architecture with few-bit ADCs can achieve a performance comparable to that obtained with fully-digital or hybrid architecture with infinite-bit ADC receiver in the low-to-medium SNR range, which is of a special importance for mmWave communications.
- We characterize the trade-off between the achievable rate and power consumption in the proposed hybrid architecture with few-bit ADC receivers. This allows us to make important conclusions about the energy efficiency of the considered hybrid architecture for different numbers of bits. This also enables us to explore the performance of the considered architecture compared with the fully-digital transceiver and the conventional hybrid architecture with full-resolution ADCs. Using numerical results and adopting a power consumption model from recent research [12], [45], we draw insights into the optimal number of quantization bits from an energy efficiency perspective. A key finding is that coarse quantization (4-5 bits) normally achieves the maximum energy efficiency. The reason is that very low quantization (1-2 bits) suffers from a severe rate loss, while high quantization (7-8 bits) has high power consumption. Hence, both of the two regimes result in very low energy efficiency.

In conclusion, this paper draws a complete picture about the generalized hybrid architectures with few-bit ADC receivers by analyzing both their achievable spectral efficiency and their energy-rate trade-off.

Notation : a is a scalar, \mathbf{a} is a vector and \mathbf{A} is a matrix. $\text{tr}(\mathbf{A})$, \mathbf{A}^* and $\|\mathbf{A}\|_F$ represents the trace, conjugate transpose and Frobenius norm of a matrix \mathbf{A} , respectively. \mathbf{I} stands for an

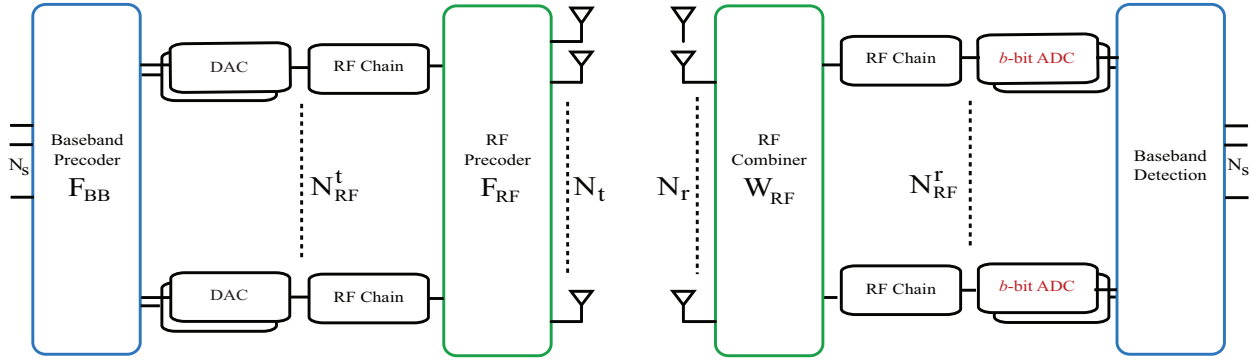


Fig. 1: A MIMO system with hybrid precoding and few-bit ADCs. The transmitter (receiver) has $N_t(N_r)$ antennas and $N_{\text{RF}}^t(N_{\text{RF}}^r)$ RF chains. the transmitter has full-precision DACs while the receiver has only few-bit low resolution ADCs.

identity matrix. $I(\mathbf{a}; \mathbf{b})$ represents the mutual information between \mathbf{a} and \mathbf{b} . $\angle(a)$ is the phase of the complex number a .

II. SYSTEM MODEL

We propose a MIMO architecture that combines hybrid analog/digital precoding and combining with few-bit ADCs, as shown in Fig. 1. The transmitter and receiver are equipped with N_t and N_r antennas, respectively. The transmitter is assumed to have N_{RF}^t RF chains with full-precision digital-to-analog converters (DACs), while the receiver employs N_{RF}^r RF chains with few-bit (1-4 bits) ADCs. Further, the number of antennas and RF chains are assumed to satisfy ($N_{\text{RF}}^t \leq N_t, N_{\text{RF}}^r \leq N_r$). The transmitter and receiver communicate via N_s data streams, with $N_s \leq \min(N_{\text{RF}}^t, N_{\text{RF}}^r)$.

Compared to the fully-digital architecture where the receiver has N_r pairs of high resolution ADCs, the proposed receiver architecture contains only N_{RF}^r pairs of few-bit ADCs, which greatly reduces both the hardware cost and power consumption. Note that the transmitter has high-resolution digital-to-analog converters (DACs) in our model. Analyzing a hybrid transceiver architecture with both low resolution ADCs and DACs is left for future work.

In this paper, we denote $\mathbf{F}_{\text{RF}} \in \mathbb{C}^{N_t \times N_{\text{RF}}^t}$ as the frequency band analog precoder and $\mathbf{F}_{\text{BB}} \in \mathbb{C}^{N_{\text{RF}}^t \times N_s}$ as the baseband digital precoder. Assuming a narrowband channel and perfect synchro-

nization, the complex baseband signal prior to combining can be written as

$$\mathbf{y} = \mathbf{H}\mathbf{F}_{\text{RF}}\mathbf{F}_{\text{BB}}\mathbf{s} + \mathbf{n}, \quad (1)$$

where \mathbf{s} is the digital baseband signal with the covariance $\mathbb{E}[\mathbf{s}\mathbf{s}^*] = \frac{P_t}{N_s}\mathbf{I}$ where P_t is the transmission power, $\mathbf{n} \sim \mathcal{CN}(0, \sigma_N^2\mathbf{I})$ is the white Gaussian noise with variance σ_N^2 .

After the analog combining, quantization and digital combining, the received signal is

$$\mathbf{v} = \mathbf{W}_{\text{BB}}^* \mathcal{Q}(\mathbf{W}_{\text{RF}}^* \mathbf{H}\mathbf{F}_{\text{RF}}\mathbf{F}_{\text{BB}}\mathbf{s} + \mathbf{W}_{\text{RF}}^* \mathbf{n}), \quad (2)$$

where $\mathbf{W}_{\text{BB}} \in \mathbb{C}^{N_{\text{RF}}^T \times N_{\text{RF}}^T}$ is the baseband combiner, $\mathbf{W}_{\text{RF}} \in \mathbb{C}^{N_{\text{r}} \times N_{\text{RF}}^T}$ is the analog combiner, and $\mathcal{Q}(\cdot)$ is a scalar quantization function which applies component-wise and separately to the real and imaginary parts.

Since this paper focuses on capacity analysis and the choice of baseband combiner \mathbf{W}_{BB} does not affect the channel capacity as long as \mathbf{W}_{BB} is invertible, we ignore the baseband combiner in this paper. Further, we assume perfect channel knowledge at the transmitter and receiver. Developing efficient channel estimation techniques for the proposed transceiver architecture is an interesting problem for future work. These techniques may leverage the previously designed channel estimation algorithms for hybrid architectures [21], [46] and MIMO systems with low-resolution ADCs [47]. We denote the signal without digital combining as

$$\mathbf{r} = \mathcal{Q}(\mathbf{W}_{\text{RF}}^* \mathbf{H}\mathbf{F}_{\text{RF}}\mathbf{F}_{\text{BB}}\mathbf{s} + \mathbf{W}_{\text{RF}}^* \mathbf{n}), \quad (3)$$

where the effective noise $\tilde{\mathbf{n}} \triangleq \mathbf{W}_{\text{RF}}^* \mathbf{n}$ has covariance $\mathbf{W}_{\text{RF}}^* \mathbf{W}_{\text{RF}}$.

With known CSI at the transmitter, the capacity of this channel is

$$C = \max_{\substack{\mathbf{F}_{\text{BB}}, \mathbf{F}_{\text{RF}}, \mathbf{W}_{\text{RF}}, \\ p(\mathbf{s}), \mathcal{Q}(\cdot)}} I(\mathbf{s}; \mathbf{r} | \mathbf{H}) \quad (4)$$

$$= \max_{\substack{\mathbf{F}_{\text{BB}}, \mathbf{F}_{\text{RF}}, \mathbf{W}_{\text{RF}}, \\ p(\mathbf{s}), \mathcal{Q}(\cdot)}} \int_{\mathbf{s}} \sum_{\mathbf{r}} p(\mathbf{s}) \Pr(\mathbf{r} | \mathbf{s}; \mathbf{H}) \log_2 \frac{\Pr(\mathbf{r} | \mathbf{s}, \mathbf{H})}{\Pr(\mathbf{r})} d\mathbf{s} \quad (5)$$

where $p(\mathbf{s})$ represents the probability distribution of \mathbf{s} , $\Pr(\mathbf{r} | \mathbf{s}; \mathbf{H})$ is the transition probability between \mathbf{s} and \mathbf{r} given \mathbf{H} , and $\Pr(\mathbf{r}) = \int_{\mathbf{s}} p(\mathbf{s}) \Pr(\mathbf{r} | \mathbf{s}, \mathbf{H}) d\mathbf{s}$. Note that the maximization is also over the quantization function $\mathcal{Q}(\cdot)$, for example, thresholds of the ADCs [39], [48]. If the simple uniform quantization is assumed, then the stepsize Δ is the only parameter in quantization function $\mathcal{Q}(\cdot)$.

III. PROBLEM FORMULATION

Since analog precoding (combining) is implemented by analog phase shifters, the entries of \mathbf{F}_{RF} (\mathbf{W}_{RF}) are limited to have same norm. The optimization problem is to maximize the mutual information between \mathbf{s} and \mathbf{r} as follows.

$$\text{P1 : } \max_{\substack{\mathbf{F}_{\text{BB}}, \mathbf{F}_{\text{RF}}, \mathbf{W}_{\text{RF}}, \\ p(\mathbf{s}), \mathcal{Q}(\cdot)}} I(\mathbf{s}; \mathbf{r} | \mathbf{H}) \quad (6)$$

$$\text{s.t. } \left| [\mathbf{F}_{\text{RF}}]_{mn} \right| = \frac{1}{\sqrt{N_t}}, \quad \forall m, n, \quad (7)$$

$$\left| [\mathbf{W}_{\text{RF}}]_{mn} \right| = \frac{1}{\sqrt{N_r}}, \quad \forall m, n, \quad (8)$$

$$\|\mathbf{F}_{\text{RF}} \mathbf{F}_{\text{BB}}\|_F^2 = N_s, \quad (9)$$

where (9) is due to the transmission power constraint, i.e., $\mathbb{E} [\|\mathbf{F}_{\text{RF}} \mathbf{F}_{\text{BB}}\|^2] = P_t$.

It is very non-trivial to solve the problem P1. First, it is hard to optimize the mutual information over so many parameters simultaneously. Second, the quantization function $\mathcal{Q}(\cdot)$ is nonlinear and also related to the input distribution $p(\mathbf{s})$ and renders it difficult to analyze the mutual information. Third, the equality constraints in (7) and (8) is non-convex and hard to deal with.

Throughout the paper, the analog precoder \mathbf{F}_{RF} is assumed to satisfy $\mathbf{F}_{\text{RF}}^* \mathbf{F}_{\text{RF}} = \mathbf{I}$. Under this assumption, the coupled power constraint (9) involving the digital and analog precoding become a simple constraint on the digital precoder \mathbf{F}_{BB} . The similar assumption also appeared in [22] where the digital and analog precoders are designed separately. In addition, we also assume that $\mathbf{W}_{\text{RF}}^* \mathbf{W}_{\text{RF}} = \mathbf{I}$ and therefore the effective noise is still white Gaussian noise. This assumption simplifies the computation of mutual information and a similar idea appeared in [49]. Further, $\mathbf{F}_{\text{RF}}^* \mathbf{F}_{\text{RF}}$ and $\mathbf{W}_{\text{RF}}^* \mathbf{W}_{\text{RF}}$ are approximately to be identity matrices when N_t and N_r is large. To sum up, we assume both the analog precoder and combiner are semi-unitary matrices.

Consequently, the optimization problem P1 is reformulated as

$$\text{P2 : } \max_{\substack{\mathbf{F}_{\text{BB}}, \mathbf{F}_{\text{RF}}, \mathbf{W}_{\text{RF}}, \\ p(\mathbf{s}), \mathcal{Q}(\cdot)}} I(\mathbf{s}; \mathbf{r} | \mathbf{H}) \quad (10)$$

$$\text{s.t. } \left| [\mathbf{F}_{\text{RF}}]_{mn} \right| = \frac{1}{\sqrt{N_t}}, \quad \forall m, n, \quad (11)$$

$$\left| [\mathbf{W}_{\text{RF}}]_{mn} \right| = \frac{1}{\sqrt{N_r}}, \quad \forall m, n, \quad (12)$$

$$\mathbf{F}_{\text{RF}}^* \mathbf{F}_{\text{RF}} = \mathbf{I}, \quad \mathbf{W}_{\text{RF}}^* \mathbf{W}_{\text{RF}} = \mathbf{I}, \quad (13)$$

$$\|\mathbf{F}_{\text{BB}}\|_F^2 \leq N_s. \quad (14)$$

In this paper, we develop two transmission strategies, including the precoding techniques, the distribution of signal \mathbf{s} , and the quantization design. We will investigate their achievable rates and show that their performance are close to optimum in certain cases.

IV. UPPER BOUND OF THE ACHIEVABLE RATE

In this section, we provide upper bounds of the achievable rate for one-bit quantization. The upper bounds are used as benchmarks for evaluating our proposed transmission methods. For multi-bit quantization, the upper bounds are unknown and left for future work.

Proposition 1. *An upper bound on the achievable rate with hybrid precoding and one-bit quantization is*

$$R^{\text{1bit,ub}} = 2N_{\text{RF}}^r \left(1 - \mathcal{H}_b \left(Q \left(\sqrt{\frac{\rho \nu_1^2}{N_{\text{RF}}^r}} \right) \right) \right), \quad (15)$$

where $\mathcal{H}_b(x) = -x \log_2 x - (1-x) \log_2 (1-x)$ is the binary entropy function, $Q(\cdot)$ is tail probability of the standard normal distribution, $\rho \triangleq \frac{P_t}{\sigma_N^2}$ is the SNR and ν_1 is the maximum singular value of the effective channel matrix $\mathbf{G} \triangleq \mathbf{W}_{\text{RF}}^* \mathbf{H} \mathbf{F}_{\text{RF}}$.

Proof: Please see the appendix. ■

The upper bound is achieved when the effective channel \mathbf{G} is full rank and has N_{RF}^r identical singular values, or equivalently, $\mathbf{G}\mathbf{G}^* = \nu_1^2 \mathbf{I}$.

At low SNR, this upper bound is approximated as

$$R^{\text{1bit,ub}} = \frac{2}{\pi} \frac{\rho \nu_1^2}{\ln 2} + o(\rho), \quad (16)$$

following the facts $Q(t) = \frac{1}{2} - \frac{1}{\sqrt{2\pi}}t + o(t^2)$ and $\mathcal{H}_b(\frac{1}{2} + t) = 1 - \frac{2}{\ln 2}t^2 + o(t^2)$. Therefore the bound increases linearly with the power at low SNR. But at high SNR, the upper bound converges to $2N_{\text{RF}}^r$ bps/Hz, which is due to the finite number of quantization output bits.

Note that the upper bound given in (15) is related to the choice of analog precoding \mathbf{W}_{RF} and \mathbf{F}_{RF} . Next, we give another bound, which is looser but independent of the analog precoding.

Corollary 1. *An upper bound of the achievable rate with hybrid precoding and one-bit quantization is*

$$\tilde{R}^{\text{1bit,ub}} = 2N_{\text{RF}}^r \left(1 - \mathcal{H}_b \left(Q \left(\sqrt{\frac{\rho \sigma_1^2}{N_{\text{RF}}^r}} \right) \right) \right), \quad (17)$$

where σ_1 is the maximum singular value of \mathbf{H} .

Proof: Under the constraint $\mathbf{W}_{\text{RF}}^* \mathbf{W}_{\text{RF}} = \mathbf{I}$ and $\mathbf{F}_{\text{RF}}^* \mathbf{F}_{\text{RF}} = \mathbf{I}$, it is proved that $\nu_1^2 \leq \sigma_1^2$ in [50, Theorem 2.2]. Therefore, we have

$$R^{\text{1bit,ub}} \leq 2N_{\text{RF}}^r \left(1 - \mathcal{H}_b \left(Q \left(\sqrt{\frac{\rho\sigma_1^2}{N_{\text{RF}}^r}} \right) \right) \right) \triangleq \tilde{R}^{\text{1bit,ub}}. \quad (18)$$

This completes the proof of Corollary 1. ■

Remark 1. For a channel with infinite-bit ADCs, a simple upper bound of the capacity is $N_{\text{RF}}^r \log_2 \left(1 + \frac{\rho\nu_1^2}{N_{\text{RF}}^r} \right)$, which is achieved when the effective channel \mathbf{G} has same singular values. Compared to (15) and (17), the bound for infinite-bit ADCs increases to infinity as the power increases to infinity.

V. ACHIEVABLE RATE WITH CHANNEL INVERSION BASED TRANSMISSION

In this section, we propose channel inversion based transmission. In this transmission method, there is no interference among data streams at the receiver and each stream is quantized separately. Therefore, the exact achievable rate of this method can be found in closed-form.

A. Channel Inversion Based Precoding Algorithm

For digital precoding design, we propose to use channel inversion precoding assuming that $N_{\text{RF}}^t \geq N_{\text{RF}}^r = N_s$. The digital precoder is

$$\mathbf{F}_{\text{BB}} = \sqrt{\frac{N_s}{\beta}} \mathbf{G}^* (\mathbf{G}\mathbf{G}^*)^{-1} \quad (19)$$

where

$$\beta = \text{tr} \left\{ \mathbf{G}^* (\mathbf{G}\mathbf{G}^*)^{-2} \mathbf{G}\mathbf{F}_{\text{RF}}^* \mathbf{F}_{\text{RF}} \right\} \quad (20)$$

such that the power constraint (9) is satisfied. As it is assumed that $\mathbf{F}_{\text{RF}}^* \mathbf{F}_{\text{RF}} = \mathbf{I}$, β is simplified to be

$$\beta = \text{tr} \left\{ (\mathbf{G}\mathbf{G}^*)^{-1} \right\}. \quad (21)$$

Since there is no interference among streams because of channel inversion precoding, each stream of data can be detected separately. The received signal is

$$\mathbf{r} = \mathcal{Q}(\mathbf{W}_{\text{RF}}^* \mathbf{H} \mathbf{F}_{\text{RF}} \mathbf{F}_{\text{BBS}} + \mathbf{W}_{\text{RF}}^* \mathbf{n}) \quad (22)$$

$$= \mathcal{Q}\left(\sqrt{\frac{N_s}{\text{tr}\{(\mathbf{G}\mathbf{G}^*)^{-1}\}}} \mathbf{s} + \mathbf{W}_{\text{RF}}^* \mathbf{n}\right). \quad (23)$$

The channel is converted to $2N_s$ parallel sub channels, each of which is a quantized real-valued single-input single-output (SISO) channel. The SNR of each sub-channel is given by

$$\text{SNR}_{\text{CI}} = \frac{\rho}{\text{tr}\{(\mathbf{G}\mathbf{G}^*)^{-1}\}}, \quad (24)$$

where $\rho \triangleq \frac{P_t}{\sigma_n^2}$.

Maximizing the SNR is equivalent to maximizing the following term

$$\eta(\mathbf{G}) \triangleq (\text{tr}\{(\mathbf{G}\mathbf{G}^*)^{-1}\})^{-1} \quad (25)$$

$$= \left(\frac{1}{\nu_1^2} + \frac{1}{\nu_2^2} + \dots + \frac{1}{\nu_{N_s}^2}\right)^{-1}, \quad (26)$$

where $\nu_1, \nu_2, \dots, \nu_{N_s}$ are the singular values of the effective channel \mathbf{G} in descending order. Therefore, \mathbf{W}_{RF} and \mathbf{F}_{RF} should be chosen to maximize the harmonic mean of the squared singular values of \mathbf{G} , or equivalently the harmonic mean of the eigenvalues of $\mathbf{G}\mathbf{G}^*$.

To maximize $\eta(\mathbf{G})$, the optimal choice of \mathbf{W}_{RF} and \mathbf{F}_{RF} are the singular vectors associated with the largest N_s singular values of \mathbf{H} [51]. Although such choice satisfies the semi-unitary constraints (13), the norm constraints (7)-(8) are violated.

In this paper, we use alternating projection algorithm [52] to find an approximate solution satisfying both the constant-norm and semi-unitary constraints. The algorithm is summarized in Algorithm 1. In steps 2a)-2b), the semi-unitary matrices $\widehat{\mathbf{W}}_{\text{RF}}$ and $\widehat{\mathbf{F}}_{\text{RF}}$ are projected to the sets of matrices satisfying the norm constraints (7)-(8), resulting in the solutions $\widetilde{\mathbf{W}}_{\text{RF}}$ and $\widetilde{\mathbf{F}}_{\text{RF}}$ respectively. Each element of $\widetilde{\mathbf{W}}_{\text{RF}}$ ($\widetilde{\mathbf{F}}_{\text{RF}}$) has the same phase of the corresponding element in $\widehat{\mathbf{W}}_{\text{RF}}$ ($\widehat{\mathbf{F}}_{\text{RF}}$) but normalized amplitude. In steps 2c)-2d), $\widetilde{\mathbf{W}}_{\text{RF}}$ and $\widetilde{\mathbf{F}}_{\text{RF}}$ are projected back to the sets of semi-unitary matrices. The projection process continues until $\frac{\|\widehat{\mathbf{F}}_{\text{RF}}^{(k)} - \widetilde{\mathbf{F}}_{\text{RF}}^{(k)}\|_F}{\sqrt{N_{\text{RF}}^t}} \left(\frac{\|\widehat{\mathbf{W}}_{\text{RF}}^{(k)} - \widetilde{\mathbf{W}}_{\text{RF}}^{(k)}\|_F}{\sqrt{N_{\text{RF}}^t}}\right)$ is smaller than a specified threshold ϵ . The convergence of the alternating projection algorithm is discussed in details in [52]. In Fig. 2, we show a typical convergence behaviour when the transmitter is assumed to have 64 antennas and 8 RF chains, while the receiver employs 8 antennas and 4

Algorithm 1 Alternating projection algorithm for analog precoding design

- 1) Initialize $\widehat{\mathbf{W}}_{\text{RF}}^{(0)} = \mathbf{U}$ and $\widehat{\mathbf{F}}_{\text{RF}}^{(0)} = \mathbf{V}$ where $\mathbf{H} = \mathbf{U}\Sigma\mathbf{V}^*$ is the singular value decomposition of \mathbf{H} . Set $k = 1$ and $\epsilon = 10^{-5}$.
 - 2) Alternating projection method
 - a) $\left[\widetilde{\mathbf{W}}_{\text{RF}}^{(k)}\right]_{mn} = \frac{1}{\sqrt{N_{\text{r}}}} \exp\left(\text{j}\angle\left(\left[\widehat{\mathbf{W}}_{\text{RF}}^{(k-1)}\right]_{mn}\right)\right), \forall m, n,$
 - b) $\left[\widetilde{\mathbf{F}}_{\text{RF}}^{(k)}\right]_{mn} = \frac{1}{\sqrt{N_{\text{t}}}} \exp\left(\text{j}\angle\left(\left[\widehat{\mathbf{F}}_{\text{RF}}^{(k-1)}\right]_{mn}\right)\right), \forall m, n,$
 - c) $\widehat{\mathbf{W}}_{\text{RF}}^{(k)} = \widetilde{\mathbf{W}}_{\text{RF}}^{(k)} \left(\left(\widetilde{\mathbf{W}}_{\text{RF}}^{(k)}\right)^* \widetilde{\mathbf{W}}_{\text{RF}}^{(k)}\right)^{-\frac{1}{2}},$
 - d) $\widehat{\mathbf{F}}_{\text{RF}}^{(k)} = \widetilde{\mathbf{F}}_{\text{RF}}^{(k)} \left(\left(\widetilde{\mathbf{F}}_{\text{RF}}^{(k)}\right)^* \widetilde{\mathbf{F}}_{\text{RF}}^{(k)}\right)^{-\frac{1}{2}},$
 - e) If the normalized distance $\frac{\|\widetilde{\mathbf{W}}_{\text{RF}}^{(k)} - \widehat{\mathbf{W}}_{\text{RF}}^{(k)}\|_F}{\sqrt{N_{\text{r}}^t}} < \epsilon$ and $\frac{\|\widetilde{\mathbf{F}}_{\text{RF}}^{(k)} - \widehat{\mathbf{F}}_{\text{RF}}^{(k)}\|_F}{\sqrt{N_{\text{r}}^t}} < \epsilon$, return $\widehat{\mathbf{W}}_{\text{RF}}^{(k)}$ and $\widehat{\mathbf{F}}_{\text{RF}}^{(k)}$; else, $k = k + 1$ and go back to step (a).
-

RF chains. Therefore, $\mathbf{F}_{\text{RF}} \in \mathbb{C}^{64 \times 8}$ and $\mathbf{W}_{\text{RF}} \in \mathbb{C}^{8 \times 4}$. Note that $\|\widetilde{\mathbf{F}}_{\text{RF}}\|_F^2 = \|\widehat{\mathbf{F}}_{\text{RF}}\|_F^2 = N_{\text{RF}}^t$ and $\|\widetilde{\mathbf{W}}_{\text{RF}}\|_F^2 = \|\widehat{\mathbf{W}}_{\text{RF}}\|_F^2 = N_{\text{RF}}^r$. So the distance is normalized by $\sqrt{N_{\text{RF}}^t}$ and $\sqrt{N_{\text{RF}}^r}$, respectively. It is seen the algorithm converges very fast, within less than 100 iterations, to a normalized distance of less than 10^{-5} .

Another choice for designing analog precoder is to assume that \mathbf{F}_{RF} and \mathbf{W}_{RF} consist of columns from the DFT matrices [1]. This is inspired by the virtual channel representation [53]. Note that the DFT matrix has constant-norm entries and orthogonal columns, therefore the norm and semi-unitary constraints of analog precoder are both satisfied. However, searching the best combination of columns has higher complexity than the alternating projection method when the number of antennas is large.

B. Rate Analysis with One-Bit Quantization

In this subsection, we focus on the special case of one-bit quantization and derive the gap between the achievable rate and the upper bound given in Proposition 1.

If one-bit ADCs are used at the receiver, the capacity of each real-valued SISO sub-channel is achieved by binary antipodal signaling and is given by [39]

$$1 - \mathcal{H}_b\left(Q\left(\sqrt{\text{SNR}_{\text{CI}}}\right)\right). \quad (27)$$

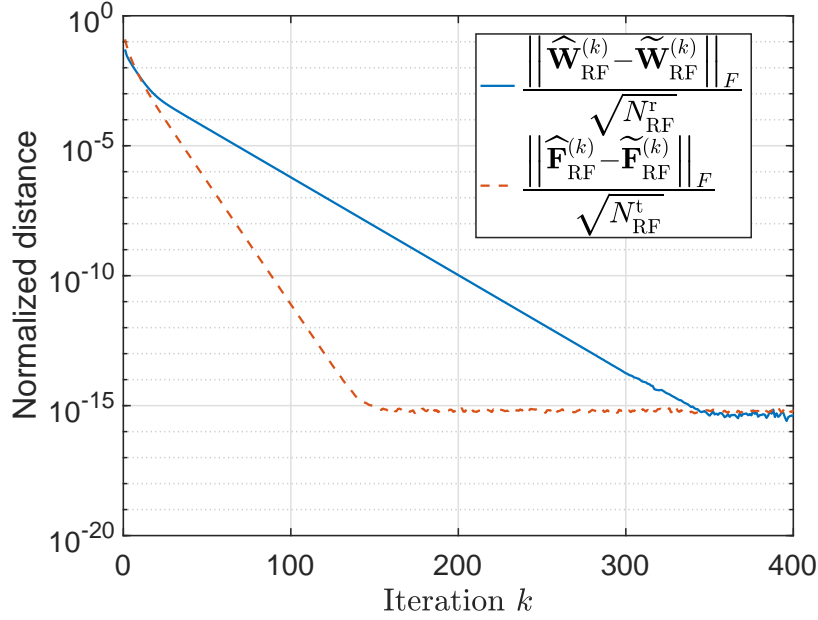


Fig. 2: This figure shows a typical convergence behaviour of the alternating projection method. The normalized error decreases exponentially with the iteration number k . In the figure, $\mathbf{F}_{\text{RF}} \in \mathbb{C}^{64 \times 8}$ and $\mathbf{W}_{\text{RF}} \in \mathbb{C}^{8 \times 4}$. Note that the floor of the normalized distance around 10^{-15} is due to the precision limitation of our computer. By default, MATLAB uses 16 digits of precision.

The total sum rate therefore is

$$R_{\text{CI}}^{\text{1bit}} = 2N_s \left(1 - \mathcal{H}_b \left(Q \left(\sqrt{\text{SNR}_{\text{CI}}} \right) \right) \right). \quad (28)$$

Next, noting that

$$\left(\frac{1}{\nu_1^2} + \frac{1}{\nu_2^2} + \cdots + \frac{1}{\nu_{N_s}^2} \right)^{-1} \geq \frac{\nu_{N_s}^2}{N_s}, \quad (29)$$

a lower bound of the SNR of the proposed precoding design is

$$\text{SNR}_{\text{CI}} \geq \frac{\rho \nu_{N_s}^2}{N_s} \triangleq \text{SNR}_{\text{lb}}. \quad (30)$$

Based on the SNR lower bound in (30), a lower bound of the achievable rate is

$$R_{\text{CI}}^{\text{1bit,lb}} = 2N_s \left(1 - \mathcal{H}_b \left(Q \left(\sqrt{\frac{\rho \nu_{N_s}^2}{N_s}} \right) \right) \right) \quad (31)$$

$$= 2N_s \left(1 - \mathcal{H}_b \left(Q \left(\sqrt{\frac{\rho \nu_1^2 \nu_{N_s}^2}{N_s \nu_1^2}} \right) \right) \right). \quad (32)$$

Comparing (32) and (15), we find that the power gap between $R^{1\text{bit,ub}}$ and $R_{\text{CI}}^{1\text{bit,lb}}$ is $10 \log_{10} \frac{\nu_1^2}{\nu_{N_s}^2}$ dB. Therefore, we conclude that compared to optimal digital precoding (which is unknown), the power loss of the channel inversion precoding is at most $10 \log_{10} \frac{\nu_1^2}{\nu_{N_s}^2}$ dB. It also implies that for a well-conditioned effective channel, the power loss is small.

Furthermore, if there is only one RF chain at the receiver, i.e., $N_{\text{RF}}^r = N_s = 1$, the achievable rate in (28) and the upper bound in (15) are exactly same and it implies that the channel capacity is achieved by the proposed transmission method.

At last, if there are more RF chains at the receiver than that at the transmitter, i.e., $N_{\text{RF}}^r > N_{\text{RF}}^t$, then only N_{RF}^t (or less than N_{RF}^t) out of N_{RF}^r receive RF chains are used, otherwise $\mathbf{G}\mathbf{G}^*$ in (19) does not have the inverse. The power consumption also decreases by turning off some receive RF chains.

C. Rate Analysis with Few-Bit Quantization

For a real-valued SISO channel with b -bit quantizer, a benchmark design was proposed in [39] where input signal are equiprobable, equispaced 2^b -PAM (pulse amplitude modulated), and quantizer thresholds are chosen to be the mid-points of the input mass point locations. Although this combination of input and quantization is suboptimal, it is shown in [39] to be close to the optimum which is obtained by high-complexity iterative algorithm. In addition, this combination is actually optimal for one-bit quantization. Therefore, in the proposed method, we assume the simple 2^{2b} -QAM signaling at the transmitter and uniform quantization at the receiver.

The channel inversion based transmission, including the analog and digital precoding design, signaling and quantization, is summarized in Transmission Method 2.

We next show an example of two-bit quantization. The derivation with multi-bit quantization is similar. The set of input signals is $\mathcal{S} = \{-\frac{3\Delta}{2}, -\frac{\Delta}{2}, \frac{\Delta}{2}, \frac{3\Delta}{2}\}$ where Δ is the stepsize. The transition probability matrix is

$$\Pr(r|s) = \begin{bmatrix} \Phi(\frac{\Delta}{2\xi}) & \Phi(\frac{3\Delta}{2\xi}) - \Phi(\frac{\Delta}{2\xi}) & \Phi(\frac{5\Delta}{2\xi}) - \Phi(\frac{3\Delta}{2\xi}) & 1 - \Phi(\frac{5\Delta}{2\xi}) \\ \Phi(\frac{-\Delta}{2\xi}) & \Phi(\frac{\Delta}{2\xi}) - \Phi(\frac{-\Delta}{2\xi}) & \Phi(\frac{3\Delta}{2\xi}) - \Phi(\frac{\Delta}{2\xi}) & 1 - \Phi(\frac{3\Delta}{2\xi}) \\ \Phi(\frac{-3\Delta}{2\xi}) & \Phi(\frac{-\Delta}{2\xi}) - \Phi(\frac{-3\Delta}{2\xi}) & \Phi(\frac{\Delta}{2\xi}) - \Phi(\frac{-\Delta}{2\xi}) & 1 - \Phi(\frac{\Delta}{2\xi}) \\ \Phi(\frac{-5\Delta}{2\xi}) & \Phi(\frac{-3\Delta}{2\xi}) - \Phi(\frac{-5\Delta}{2\xi}) & \Phi(\frac{-\Delta}{2\xi}) - \Phi(\frac{-3\Delta}{2\xi}) & 1 - \Phi(\frac{-\Delta}{2\xi}) \end{bmatrix} \begin{matrix} s = -\frac{3\Delta}{2} \\ s = -\frac{\Delta}{2} \\ s = \frac{\Delta}{2} \\ s = \frac{3\Delta}{2} \end{matrix} \quad (33)$$

$$r = -\frac{3\Delta}{2} \quad r = -\frac{\Delta}{2} \quad r = \frac{\Delta}{2} \quad r = \frac{3\Delta}{2}$$

Transmission Method 2 Channel Inversion Based Transmission Method

1) **Analog precoding design:** Find the approximate solution $\overline{\mathbf{W}}_{\text{RF}}$ and $\overline{\mathbf{F}}_{\text{RF}}$ by the alternating projection shown in Algorithm 1.

2) **Digital precoding design:**

a) Compute the effective channel $\overline{\mathbf{G}} \triangleq \overline{\mathbf{W}}_{\text{RF}}^* \mathbf{H} \overline{\mathbf{F}}_{\text{RF}}$.

b) Set the digital precoder \mathbf{F}_{BB} as

$$\mathbf{F}_{\text{BB}} = \sqrt{\frac{N_s}{\text{tr} \left\{ \left(\overline{\mathbf{G}} \overline{\mathbf{G}}^* \right)^{-1} \right\}}} \overline{\mathbf{G}}^* \left(\overline{\mathbf{G}} \overline{\mathbf{G}}^* \right)^{-1}.$$

3) **Signaling:** s is chosen to be 2^{2b} -QAM symbols.

4) **Quantization:** Uniform quantization.

where ξ^2 denotes the noise variance and $\Phi(\cdot)$ is the cumulative distribution function of the standard normal distribution. The transition probability matrix of higher resolution ADCs could be obtained similarly.

The SNR of each sub-channel must be equal to the value given in (24). Therefore,

$$\frac{1}{2^{b+1}} \left(\Delta^2 + (3\Delta)^2 + \dots + ((2^b - 1) \Delta)^2 \right) / \xi^2 = \text{SNR}_{\text{CI}} \quad (34)$$

$$\frac{1}{2^{b+1}} \frac{1}{3} 2^{b-1} (2^{2b} - 1) \frac{\Delta^2}{\xi^2} = \text{SNR}_{\text{CI}} \quad (35)$$

$$\frac{\Delta}{\xi} = \sqrt{\frac{12 \text{SNR}_{\text{CI}}}{2^{2b} - 1}} \quad (36)$$

where (35) is from the fact that $1^2 + 3^2 + \dots + (2n - 1)^2 = \frac{1}{3}n(4n^2 - 1)$.

The achievable rate can therefore be computed as

$$R_{\text{CI}}^{\text{bit}} = 2N_s \sum_s \sum_r \Pr(s) \Pr(r|s) \log \frac{\Pr(r|s)}{\Pr(r)} \quad (37)$$

$$= 2N_s \sum_s \sum_r \Pr(s) \Pr(r|s) \log \frac{\Pr(r|s)}{\sum_{s'} \Pr(s') \Pr(r|s')} \quad (38)$$

$$\stackrel{(a)}{\leq} 2N_s \sum_s \sum_r \frac{1}{2^b} \Pr(r|s) \log \frac{\Pr(r|s)}{\frac{1}{2^b} \sum_{s'} \Pr(r|s')} \quad (39)$$

$$= 2N_s \left(b + \frac{1}{2^b} \sum_s \sum_r \Pr(r|s) \log \frac{\Pr(r|s)}{\sum_{s'} \Pr(r|s')} \right), \quad (40)$$

where (a) follow from that the equal transmission probability $\Pr(s) = \frac{1}{2^b}$. The achievable rate in (40) is complicated and does not provide us with enough intuition. A simple lower bound of (40) can be found by Fano's inequality [54, Section 2.10]. The conditional entropy is upper bounded by

$$\mathcal{H}_b(s|r) \leq \mathcal{H}_b(P_e) + P_e \log(|\mathcal{S}| - 1), \quad (41)$$

where P_e is the error probability. Hence, the mutual information between s and r is

$$I(s; r) = \mathcal{H}_b(s) - \mathcal{H}_b(s|r) \quad (42)$$

$$\geq b - \mathcal{H}_b(P_e) - P_e \log(2^b - 1). \quad (43)$$

A lower bound of the sum rate of $2N_s$ sub-channels therefore is

$$R_{\text{CI}}^{\text{bit,lb}} = 2N_s (b - \mathcal{H}_b(P_e) - P_e \log(2^b - 1)), \quad (44)$$

where the error probability P_e for 2^b -PAM signaling is [55]

$$P_e = 2 \left(1 - \frac{1}{2^b}\right) Q\left(\frac{\Delta}{2\xi}\right) \quad (45)$$

$$= 2 \left(1 - \frac{1}{2^b}\right) Q\left(\sqrt{\frac{3 \text{SNR}_{\text{CI}}}{2^{2b} - 1}}\right). \quad (46)$$

From (44), we find that the as SNR_{CI} increases, P_e decreases to zero and $R_{\text{CI}}^{\text{bit,lb}}$ converges to $2N_s b$ bps/Hz. In addition, note that for the one-bit case, $P_e = Q(\sqrt{\text{SNR}_{\text{CI}}})$ and therefore (44) degrades to (28).

VI. ACHIEVABLE RATE WITH SINGULAR VALUE DECOMPOSITION BASED TRANSMISSION

The channel inversion precoding generally works well at high SNR and has poor performance at low SNR. In the second transmission method, we use the singular value decomposition (SVD) digital precoding. Since the interference between each steams can not be completely eliminated before quantization as in the channel inversion case, the exact achievable rate is unknown. We therefore choose to apply the additive quantization noise model (AQNM) [32], [35], [56], which is accurate enough at low SNR, to find a lower bound of the achievable rate.

Applying the additive quantization noise model, the equivalent channel is

$$\mathbf{r} = (1 - \eta_b) (\mathbf{G}\mathbf{F}_{\text{BBS}} + \mathbf{W}_{\text{RF}}^* \mathbf{n}) + \mathbf{n}_Q, \quad (47)$$

where η_b is the distortion factor for b -bit ADC defined as $\eta_b = \frac{\mathbb{E}[(\mathbf{Q}(y)-y)^2]}{\mathbb{E}[|y|^2]}$ and \mathbf{n}_Q is the quantization noise with the variance $\eta_b(1-\eta_b)\text{diag}\left\{\frac{P_s}{N_s}\mathbf{G}\mathbf{F}_{\text{BB}}\mathbf{F}_{\text{BB}}^*\mathbf{G}^* + \sigma_N^2\mathbf{I}\right\}$.

Assuming \mathbf{s} is Gaussian distributed and the quantization noise is the worst case of Gaussian distributed, a lower bound of the achievable rate is

$$R_{\text{AQNM}} = \log_2 \left| \mathbf{I} + (1-\eta_b)\frac{\rho}{N_s}\mathbf{F}_{\text{BB}}^*\mathbf{G}^* \left(\mathbf{I} + \eta_b \text{diag} \left\{ \frac{\rho}{N_s}\mathbf{G}\mathbf{F}_{\text{BB}}\mathbf{F}_{\text{BB}}^*\mathbf{G}^* \right\} \right)^{-1} \mathbf{G}\mathbf{F}_{\text{BB}} \right|. \quad (48)$$

At low SNR, the achievable rate is approximated to be

$$R_{\text{AQNM}} = \log_2 \left| \mathbf{I} + (1-\eta_b)\frac{\rho}{N_s}\mathbf{F}_{\text{BB}}^*\mathbf{G}^*\mathbf{G}\mathbf{F}_{\text{BB}} \right| + o(\rho) \quad (49)$$

$$= \frac{(1-\eta_b)\rho}{N_s \ln 2} \text{tr} \{ \mathbf{F}_{\text{BB}}^*\mathbf{G}^*\mathbf{G}\mathbf{F}_{\text{BB}} \} + o(\rho). \quad (50)$$

To maximize the term $\frac{1}{N_s}\text{tr} \{ \mathbf{G}\mathbf{F}_{\text{BB}}\mathbf{F}_{\text{BB}}^*\mathbf{G}^* \}$ under the constraint $\|\mathbf{F}_{\text{BB}}\|_F^2 \leq N_s$, the optimal choice of \mathbf{F}_{BB} is the eigenmode beamforming, i.e.,

$$N_s = 1, \quad \text{and} \quad \mathbf{F}_{\text{BB}} = \mathbf{v}_1, \quad (51)$$

where \mathbf{v}_1 is the right singular vector corresponding to the largest singular value of \mathbf{G} . The resulting rate is

$$R_{\text{AQNM}} = \frac{(1-\eta_b)\rho\nu_1^2}{\ln 2} + o(\rho). \quad (52)$$

For one-bit quantization, $\eta_1 = 1 - \frac{2}{\pi}$ and the rate is

$$R_{\text{AQNM}} = \frac{2}{\pi} \frac{\rho\nu_1^2}{\ln 2} + o(\rho). \quad (53)$$

Notice that the upper bound of one-bit quantized channel at low SNR given in (16) is achieved by eigenmode beamforming.

For higher SNR, the optimal \mathbf{F}_{BB} maximizing the rate R_{AQNM} in (48) is unknown. We therefore use the conventional SVD precoding and waterfilling power allocation as done in [31], [36]. The baseband digital precoder is

$$\mathbf{F}_{\text{BB}} = \mathbf{V} \text{diag} \{ \sqrt{\mathbf{p}} \}, \quad (54)$$

where \mathbf{V} is obtained from the singular value decomposition of the matrix \mathbf{G} , i.e., $\mathbf{G} = \mathbf{U}\mathbf{\Sigma}\mathbf{V}^*$ and \mathbf{p} denotes the power allocation factor obtained from the waterfilling method.

For the analog precoding and combining, the optimal \mathbf{F}_{RF} and \mathbf{W}_{RF} the rate in (48) are unknown. We adopt the same alternating projection method in Algorithm 1 to find a suboptimal

solution. As a result, the analog precoding is designed by alternating projection method with initial values obtain by SVD of the channel and the the digital precoding is got by SVD of the baseband channel. The proposed SVD based design is summarized in Transmission Method 3.

Transmission Method 3 SVD Based Transmission Method

- 1) **Analog precoding design:** Find the approximate solution $\overline{\mathbf{W}}_{\text{RF}}$ and $\overline{\mathbf{F}}_{\text{RF}}$ by the alternating projection method shown in Algorithm 1.
 - 2) **Digital precoding design:**
 - a) Compute the effective channel $\overline{\mathbf{G}} \triangleq \overline{\mathbf{W}}_{\text{RF}}^* \mathbf{H} \overline{\mathbf{F}}_{\text{RF}}$.
 - b) Set the digital precoder \mathbf{F}_{BB} by SVD of $\overline{\mathbf{G}}$ and waterfilling method.
 - 3) **Signaling:** \mathbf{s} is chosen to follow Gaussian signaling.
 - 4) **Quantization:** The thresholds of ADC are determined by Max-Lloyd algorithm [57], [58] which minimizes the MSE of Gaussian distributed input.
-

Last, we show why the AQNM model is not accurate enough at high SNR to model the quantization channel. At high SNR, R_{AQNM} converges as follows.

$$R_{\text{AQNM}} \approx \log_2 \left| \mathbf{I} + \frac{1 - \eta_b}{\eta_b} \mathbf{F}_{\text{BB}}^* \mathbf{G}^* (\text{diag} \{ \mathbf{G} \mathbf{F}_{\text{BB}} \mathbf{F}_{\text{BB}}^* \mathbf{G}^* \})^{-1} \mathbf{G} \mathbf{F}_{\text{BB}} \right| \quad (55)$$

$$= \log_2 \left| \mathbf{I} + \frac{1 - \eta_b}{\eta_b} \mathbf{A}^* \text{diag} \left\{ \frac{1}{\|\mathbf{a}_i\|} \right\} \text{diag} \left\{ \frac{1}{\|\mathbf{a}_i\|} \right\} \mathbf{A} \right| \quad (56)$$

$$= \log_2 \left| \mathbf{I} + \frac{1 - \eta_b}{\eta_b} \tilde{\mathbf{A}}^* \tilde{\mathbf{A}} \right| \quad (57)$$

$$= \sum_{i=1}^{N_s} \log_2 \left(1 + \frac{1 - \eta_b}{\eta_b} \lambda_i (\tilde{\mathbf{A}}^* \tilde{\mathbf{A}}) \right) \quad (58)$$

where $\mathbf{A} \triangleq \mathbf{G} \mathbf{F}_{\text{BB}}$ is a Hermitian matrix, \mathbf{a}_i is the i -th column of \mathbf{A} , and $\tilde{\mathbf{A}}$ is obtained by normalizing each each row of \mathbf{A} . Since each row of $\tilde{\mathbf{A}}$ has unit norm, then

$$\sum_{i=1}^{N_s} \lambda_i (\tilde{\mathbf{A}}^* \tilde{\mathbf{A}}) = \text{tr} (\tilde{\mathbf{A}}^* \tilde{\mathbf{A}}) = N_s. \quad (59)$$

Therefore, we have

$$R_{\text{AQNM}} \stackrel{(a)}{\leq} N_s \log_2 \left(1 + \frac{1 - \eta_b}{\eta_b} \right) \quad (60)$$

$$= N_s \log_2 \frac{1}{\eta_b}, \quad (61)$$

where (a) follows from Jensen's inequality and that $\log_2(1+x)$ is concave in x . When the ADC resolution b is large ($b \geq 3$), the distortion factor η_b can be approximated as [59]

$$\eta_b \approx \frac{\pi\sqrt{3}}{2}2^{-2b}. \quad (62)$$

As a result, the rate obtained by AQNM model is upper bounded by

$$R_{\text{AQNM}} \leq 2N_s b - N_s \log_2 \frac{\pi\sqrt{3}}{2} \quad (63)$$

$$\approx 2N_s b - 1.44N_s. \quad (64)$$

However, we know the achievable rate of quantized MIMO channel is upper bounded by $2N_s b$ bps/Hz and the channel inversion method can achieve the bound at high enough SNR as shown in (44). Therefore, the AQNM is not an accurate model at high SNR. The reason is threefold. First, the input signal \mathbf{s} is assumed to be follow suboptimal continuous Gaussian. Second, the quantization noise is assumed to be the worst-case Gaussian noise. Third, the Max-Lloyd quantizer minimizing the MSE is not necessarily optimum for maximizing the channel capacity.

VII. SIMULATION RESULTS

We evaluate the performance of proposed methods in a mmWave MIMO channel with large antenna arrays and limited number of transmit and receive RF chains. According to measurement results [60], [61], the number of clusters tends to be lower in the mmWave band compared with lower frequencies. The mmWave channel will mostly consist of the line-of-sight (LOS) and a few NLOS clusters. In the simulations, the wireless channel is assumed to have 4 clusters, each of which consists of 5 rays. The angle spread is 7.5 degrees. These numbers are chosen according to the urban macro (UMa) NLOS channel measurement results at 28 GHz given in the white paper [62]. The results are obtained by averaging over 100 channel realizations.

A. Achievable Rates

In this subsection, we evaluate the achievable rates of the proposed architecture by numerical simulations. The transmitter is assumed to have $N_t = 64$ antennas and $N_{\text{RF}}^t = 8$ RF chains, while the receiver employs $N_r = 8$ antennas. The number of data streams is assumed to same as the number of receive RF chains, i.e., $N_s = N_{\text{RF}}^r$.

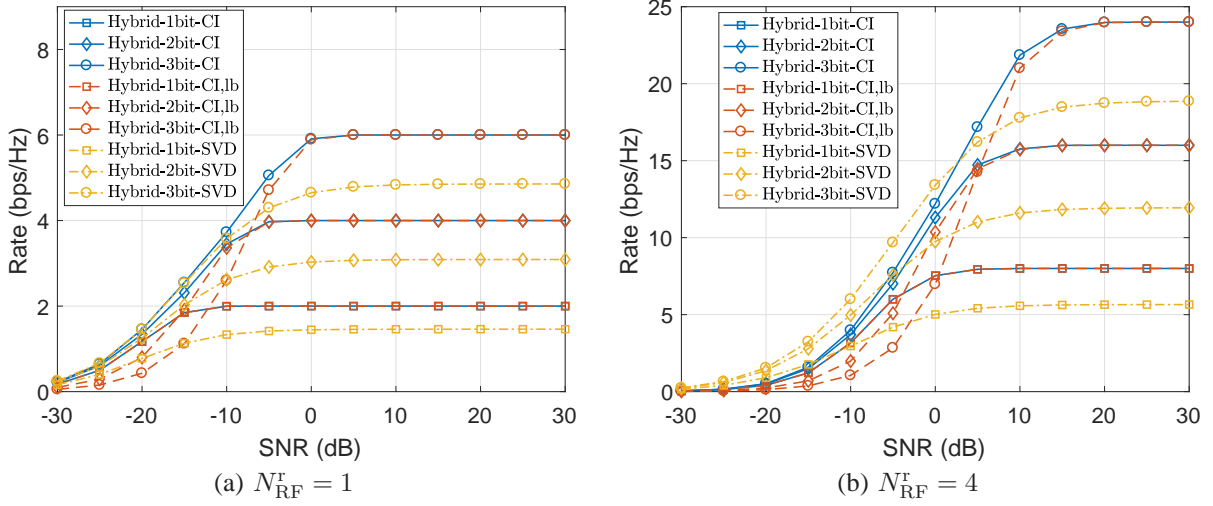


Fig. 3: This figure shows rates versus SNR of different transmission methods. The transmitter is assumed to have 64 antennas and 8 RF chains. The receiver employs 8 antennas. In Fig. (a), the receiver has 1 RF chains while in Fig. (b), the receiver has 4 RF chains.

Fig. 3 shows the achievable rates when the receiver has 1 and 4 RF chains, respectively. In Fig. 3a, it is seen that when there is only one RF chains at the transmitter, the channel inversion and SVD method has close performance at low SNR. At high SNR, however, the channel inversion method achieves the rate $2b$ bps/Hz while the rate of SVD method saturates to $\log_2 \frac{1}{\eta_b}$ which is about 1.46, 3.09, 4.86 bps/Hz for $b = 1, 2, 3$, respectively. In Fig. 3b, another case when $N_{\text{RF}}^T = 4$ is shown. It is found that although at high SNR the channel inversion method achieves larger rate than SVD method, its performance at low SNR is much worse. The reason is that since the channel has only 4 clusters, the fourth largest singular value ν_4 is small and the power loss $\log_2 \frac{\nu_1^2}{\nu_4^2}$ is large. Last, the lower bound provided in (44) is also plotted. It is seen that the lower bound is tight for 1-bit ADC case. For other cases, the lower bound is tight at high SNR.

Fig. 4 compares the achievable rate of fully-digital and hybrid architecture. The rate of hybrid architecture is the maximum of the CI and SVD method. The gap between the curves of “Digital- b bit” and “Hybrid- b bit” represents the loss due to limited number of RF chains while the gap between the curves of “ ∞ bit” and “ b bit” is the loss due to low resolution ADCs. It is seen that the digital architecture is much better than the hybrid architecture with only one RF chain because the hybrid architecture can only support single stream transmission while the digital architecture

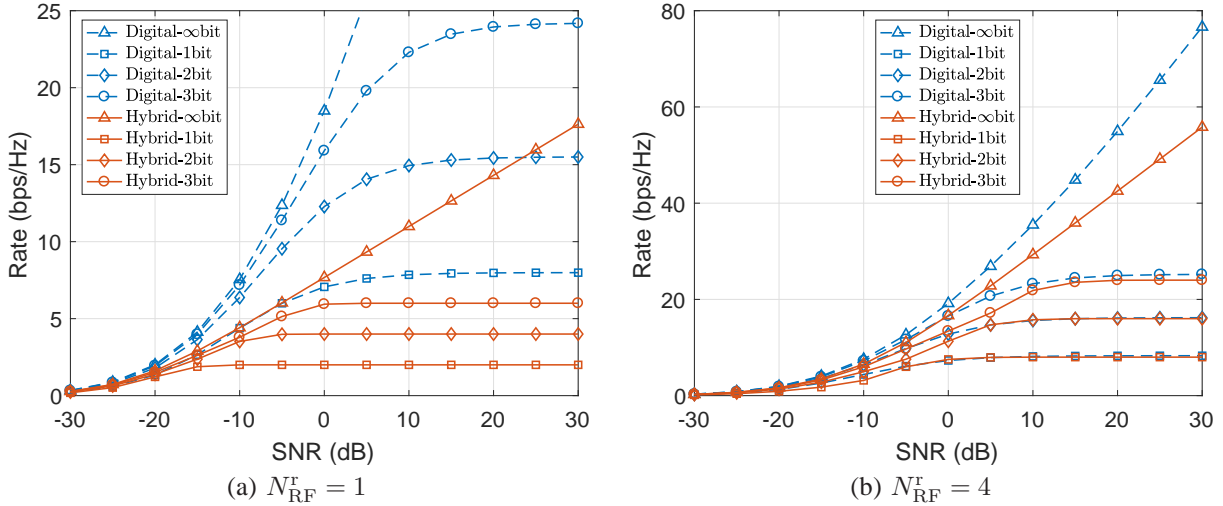


Fig. 4: This figure shows rates versus SNR of different transmission methods. The transmitter is assumed to have 64 antennas and 8 RF chains. The receiver employs 8 antennas. In Fig. (a), the receiver has 1 RF chains while in Fig. (b), the receiver has 4 RF chains.

can support at most 8 streams simultaneously. However, when there are 4 receive RF chains in the hybrid architecture, the gap between these two architecture is small since the channel has 4 clusters. Last, we can see the loss due to low resolution ADCs is small at low and medium SNRs. For example, the gap between the curve “Hybrid-∞bit” and “Hybrid-3bit” is less than 3 dB when the SNR is less than 10 dB in Fig. 4b.

Fig. 5 shows the achievable rate with respect to the ADC resolution. First, as expected, the rates of the finite-bit ADC receiver increase with resolution. Second, with multi-bit ADCs (5-bit when $\text{SNR} = -10$ dB and 7-bit when $\text{SNR} = 10$ dB), the SVD method achieves the performance similar to that of hybrid architecture with ∞-bit ADCs. This implies that high resolution ADC do not provide much gain compared to the few-bit ADC when the SNR is low. Third, when the ADC resolution is low, channel inversion method is better than the SVD method while with high resolution quantization, the SVD method is better. This is reasonable since with high resolution ADC, the channel is close to the one without quantization and in a unquantized channel, SVD method is optimum.

Fig. 6 presents the achievable rates versus the number of RF chains at the receiver. First, we find that the rate of SVD method always increases with N_{RF}^T . Second, at low SNR (-10 dB),

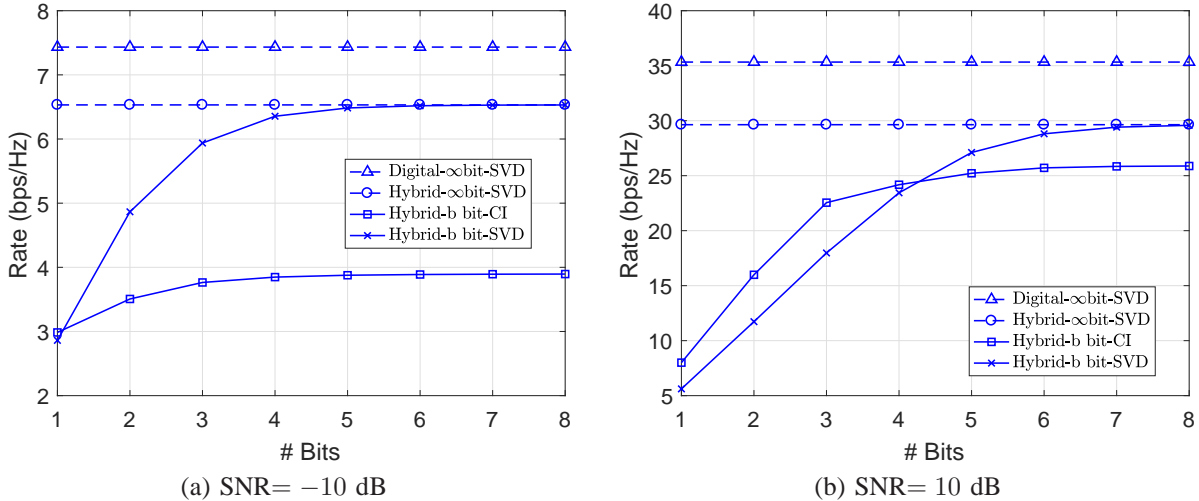


Fig. 5: This figure shows rates versus ADC resolution for different transmission methods. The transmitter is assumed to have 64 antennas and 8 RF chains. The receiver employs 8 antennas and 4 RF chains. In Fig. (a), the SNR is -10 dB while in Fig. (b), the SNR is 10 dB.

the channel inversion method achieve the largest rate when $N_{\text{RF}}^{\text{t}} = 2$. This means at low SNR, it is better to turn off some RF chains and transmit fewer number of steams. Note that the power consumption also decreases by turning off some RF chains. Third, we find that compared to fully-digital architecture where $N_{\text{RF}}^{\text{t}} = N_{\text{t}} = 64$ and $N_{\text{RF}}^{\text{r}} = N_{\text{r}} = 8$, the hybrid architecture with limited number of RF chains ($N_{\text{RF}}^{\text{t}} = 8$ and $N_{\text{RF}}^{\text{r}} = 2$) and low resolution ADCs (4-bit) incurs about 20%-30% spectral efficiency loss. As shown in the next subsection, however, the energy efficiency of the proposed receiver is much higher than the fully-digital architecture.

B. Energy efficiency

In this subsection, we evaluate the performance of the different receiver architectures by investigating the trade-off between their achievable rates and power consumption. First, we formulate a generic power consumption model for the hybrid architecture with low-resolution ADCs. Then, we use this model in the performance evaluation. Consider the system model in Fig. 1 with a b -bit ADC receiver having N_{r} antennas and N_{RF}^{r} RF chains. Let P_{LNA} , P_{PS} , P_{RFchain} , P_{ADC} , P_{BB} denote the power consumption in the LNA, phase shifter, RF chains, ADC, and baseband processor, respectively. Then, the consumed power by the hybrid combining receiver

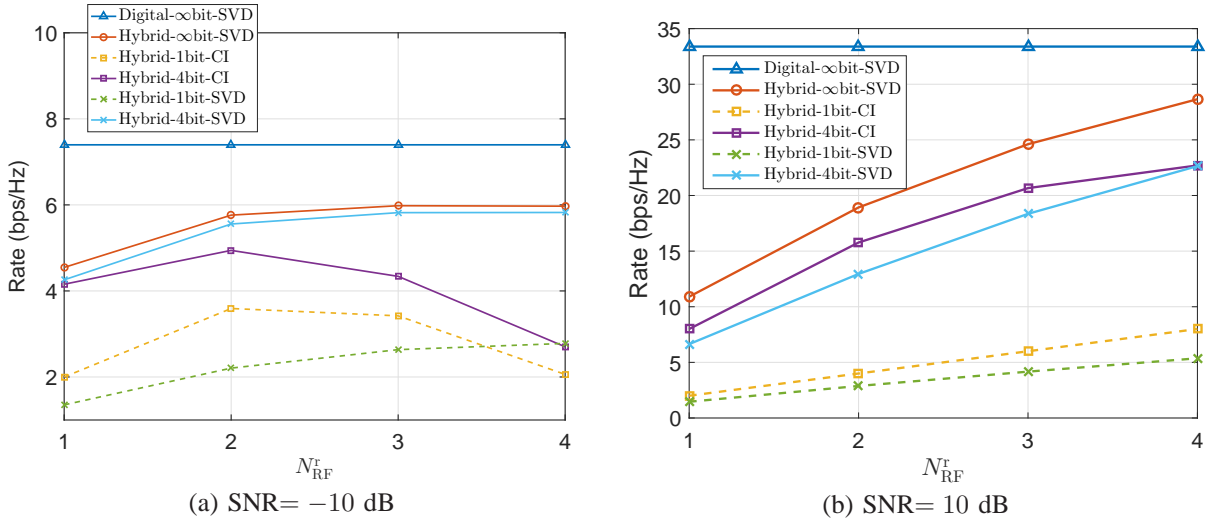


Fig. 6: This figure shows rates versus the number of receive RF chains for different transceiver architecture and transmission methods. The transmitter is assumed to have 64 antennas and 8 RF chains, while the receiver employs 8 antennas. In Fig. (a), the SNR is -10 dB while in Fig. (b), the SNR is 10 dB.

in Fig. 1 can be approximated as [63]

$$P_{\text{tot}} = N_r P_{\text{LNA}} + N_{\text{RF}}^r (N_r P_{\text{PS}} + P_{\text{RFchain}} + 2P_{\text{ADC}}) + P_{\text{BB}}, \quad (65)$$

where the power consumed by ADCs can be further expressed in terms of the number of bits as

$$P_{\text{ADC}} = FOM_W \cdot f_s \cdot 2^b, \quad (66)$$

where f_s is the Nyquist sampling rate, b is the number of bits, and FOM_W is Walden's figure-of-merit for evaluating ADC's power efficiency with resolution and speed [12], [28],

Next, we present some simulation results in Figs. 7-8 that illustrate the power consumption-rate trade-off of the hybrid combining receiver for different number of RF chains and ADC quantization bits at the receiver. In these simulations, we adopt the same clustered channel model, and consider the system model in Section II with a transmitter having 64 antennas and 8 RF chains, and a receiver deploying 8 antennas.

First, we plot in Fig. 7 the power consumption versus the achievable rate for the fully-digital and proposed hybrid architecture with few-bit ADC receivers. The power consumption in the different receivers are calculated based on the power model in (65)-(66). The consumed power

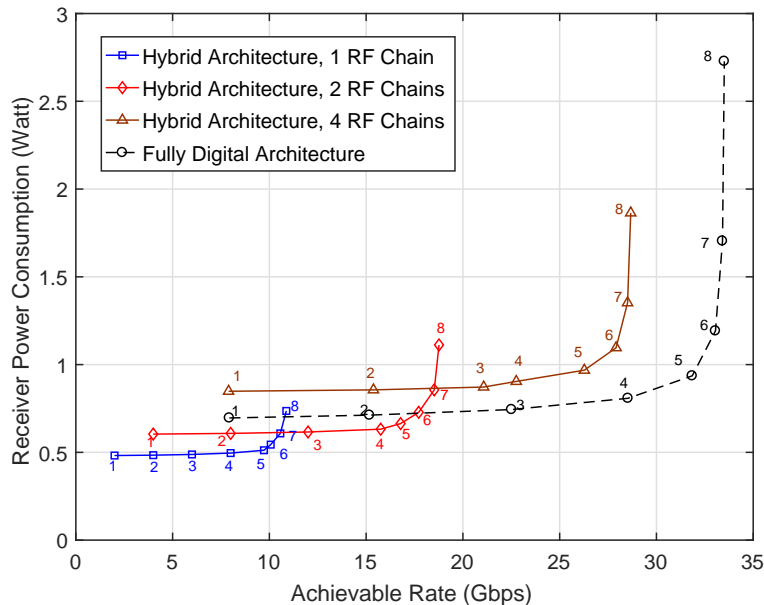


Fig. 7: Trade-off between the achievable rate and power consumption for hybrid combiners with different number of RF chains and ADC bits. The results also include the fully-digital architecture with finite-bit ADCs. The transmitter is assumed to have 64 antennas and 8 RF chains, while the receiver employs 8 antennas and 1, 2 or 4 RF chains. The SNR is 10 dB and the bandwidth is 1 GHz.

in the RF components are assumed to be $P_{\text{LNA}} = 20$ mW, $P_{\text{PS}} = 10$ mW, $P_{\text{RFchain}} = 40$ mW, $P_{\text{BB}} = 200$ mW [63], [64]. For the ADCs, we adopt the power consumption model in (66) with $FOM_W = 500$ fJ/conversion-step, which is a typical achievable value at 1 GHz [12], [65]¹.

The achievable rate for the hybrid architecture with few-bit ADCs in Fig. 7 is calculated as the maximum of the two achievable rate expressions in (40) and (48) for CI and SVD based precoding. Several important insights can be obtained from Fig. 7. First, for all the four cases in the figure, the achievable rate significantly increases when the number of bits increases from 1 to 4 – 5 bits, with a negligible increase in the receiver power consumption. This implies that with these system configurations, having 4 – 5 bits ADC’s can lead to a better trade-off between the rate and power consumption compared with having 1-bit ADC receivers. Next, going from

¹The minimum achievable value of FOM_W can be as low as 5 fJ/conversion-step as shown in the Figure “Walden FOM vs. Speed” in [12].

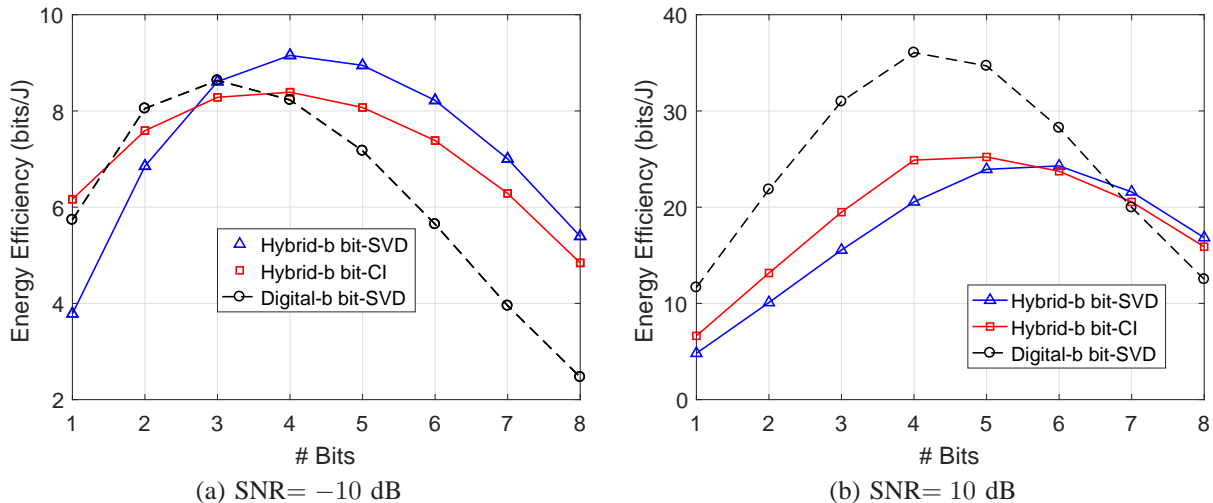


Fig. 8: Energy efficiency of the digital and hybrid architecture with few-bit ADC receivers for different numbers of bits. The transmitter is assumed to have 64 antennas and 8 RF chains, while the receiver employs 8 antennas and 2 RF chains. In Fig. (a), the SNR is -10 dB while in Fig. (b), and the SNR is 10 dB.

4 – 5 bits to 7 – 8 bits for the ADCs in the hybrid architectures slightly improves the achievable spectral efficiency, but with significantly more power consumption. This means that 4 – 5 ADC bits can be better than 7 – 8 ADC bits when investigating the rate-power consumption trade-off. Second, it is found that among the four cases considered, the hybrid one with 1 RF chain gives the best power-rate trade-off when the rate is less than 11 Gbps, the hybrid one with 2 RF chains gives the best trade-off when the rate is between 11 Gbps and 18 Gbps, and the fully-digital architecture is best when the rate is larger than 18 Gbps. Third, when there are 4 RF chains, the performance of hybrid architecture is dominated by that of the fully-digital architecture. To achieve the same rate, the power consumption of hybrid receiver with 4 RF chains is always larger than of fully-digital one because of the high power consumption of the large number of analog phase shifters.

Based on the observations made from Fig. 7, we investigate the energy efficiency of the different receiver architectures in Fig. 8. The energy spectral efficiency η_{EE} is defined as

$$\eta_{EE} = \frac{R W}{P_{\text{tot}}} \text{bits/Joule}, \quad (67)$$

where R is the achievable spectral efficiency and W is the transmission bandwidth. The channel

and system models adopted in Fig. 8a-Fig. 8b are similar to that in Fig. 7 with 2 RF chains used at the receiver and with $W = 1$ GHz bandwidth. In Fig. 8a, the energy efficiency of the few-bit ADC hybrid architecture is plotted for two different precoding techniques versus the number of ADC bits at SNR= -10 dB. The result is compared with the energy efficiencies of the fully-digital transceiver. Fig. 8a shows that the number of bits maximizing the energy efficiency is finite and equals to 4 bits. This maximum energy efficiency is achieved with the SVD precoding in (48). It is worth noting from Fig. 8a that the choice of the precoding technique depends on the number of ADC quantization bits. While the channel inversion achieves a better energy efficiency with 1 – 2 ADC bits, SVD precoding can lead to a better energy efficiency for higher numbers of ADC quantization bits. Fig. 8b has the same comparison in Fig. 8a with the only difference of operating at SNR=10 dB. The energy efficiency trends in Fig. 8b are similar to that in Fig. 8a with the main difference that the maximum energy efficiency is achieved with the channel inversion precoding in (40). This implies that determining the precoding techniques should take the SNR into consideration. We note though the 4 bits for the ADC quantization still achieves the optimal energy efficiency. Further, Fig. 8a-Fig. 8b also show that energy efficiency of the proposed few-bit ADC hybrid architecture can be much better than that of the fully-digital architectures that employ high resolution ADCs. The reason is that the ADC will dominate the power consumption when the resolution is high and hybrid architecture saves power by reducing the number of high-resolution ADCs.

VIII. CONCLUSION

In this paper, we derived the achievable spectral efficiency and energy-rate trade-off of a generalized hybrid architecture with few-bit ADC receivers. First, we considered channel inversion and SVD precoding based transmission methods and derived their achievable rates. The transmission methods include three elements: the design of analog and digital precoding, the choice of the transmit signal distribution and the setup of quantizer. Simulation results showed that at the low and medium SNRs, the proposed architecture and precoding can achieve a comparable rate to the fully-digital solution. Second, we explored the trade-off between the achievable rate and the power consumption, which is particularly important in massive MIMO and mmWave systems. Adopting energy efficiency as a performance metric, the proposed hybrid architecture with few-bit ADC receiver is compared with the fully-digital transceiver and the conventional hybrid

architecture with full-resolution ADCs. Numerical results showed that the generalized hybrid architecture with coarse ADC quantization achieves a potential energy efficiency gain compared to the other architectures. The results illustrated that coarse ADC quantization with 4 – 5 bits normally achieves the maximum energy efficiency in various system configurations.

APPENDIX A

PROOF OF PROPOSITION 1

The proof is similar to the proof of [17, Proposition 4]. The channel without any constraint on digital precoding and combining is,

$$\mathbf{r} = \text{sgn}(\mathbf{W}_{\text{RF}}^* \mathbf{H} \mathbf{F}_{\text{RF}} \mathbf{x} + \mathbf{W}_{\text{RF}}^* \mathbf{n}). \quad (68)$$

We want to find an upper bound of the mutual information $I(\mathbf{r}; \mathbf{x})$ subject to the power constraint $\mathbb{E}[\|\mathbf{F}_{\text{RF}} \mathbf{x}\|^2] \leq P_t$.

First, we have,

$$I(\mathbf{r}; \mathbf{x}) = \mathcal{H}(\mathbf{r}) - \mathcal{H}(\mathbf{r}|\mathbf{x}) \quad (69)$$

$$\stackrel{(a)}{\leq} 2N_{\text{RF}}^T - \mathcal{H}(\mathbf{r}|\mathbf{x}), \quad (70)$$

where inequality (a) follows from that there are at most $2N_{\text{RF}}^T$ quantization outputs.

Next, we derive a lower bound of $\mathcal{H}(\mathbf{r}|\mathbf{x})$. For a given transmitted signal $\mathbf{x} = \mathbf{x}'$, denote $\mathbf{z}' = \mathbf{W}_{\text{RF}}^* \mathbf{H} \mathbf{F}_{\text{RF}} \mathbf{x}'$ and $\tilde{\mathbf{z}}' = [\text{Re}(\mathbf{z}')^T, \text{Im}(\mathbf{z}')^T]^T$. The conditional entropy of \mathbf{r} given $\mathbf{x} = \mathbf{x}'$ is,

$$\mathcal{H}(\mathbf{r}|\mathbf{x} = \mathbf{x}') \stackrel{(a)}{=} \sum_{j=1}^{N_{\text{RF}}^T} \mathcal{H}(\mathbf{r}_j|\mathbf{x}') \quad (71)$$

$$\stackrel{(b)}{=} \sum_{j=1}^{2N_{\text{RF}}^T} \mathcal{H}_b \left(Q \left(\sqrt{\frac{2}{\sigma_{\text{N}}^2}} \tilde{\mathbf{z}}'_j \right) \right) \quad (72)$$

$$\stackrel{(c)}{=} \sum_{j=1}^{2N_{\text{RF}}^T} \mathcal{H}_b \left(Q \left(\sqrt{\frac{2(\tilde{\mathbf{z}}'_j)^2}{\sigma_{\text{N}}^2}} \right) \right) \quad (73)$$

where (a) follows from that the effective noise $\mathbf{W}_{\text{RF}}^* \mathbf{n}$ has independent entries, (b) follows from that the in-phase and quadrature parts of the effective noise are independent and Gaussian distributed with variance $\frac{\sigma_{\text{N}}^2}{2}$, (c) follows from that $\mathcal{H}_b(Q(x))$ is an even function of x . Next,

noting that

$$\sum_{j=1}^{2N_{\text{RF}}^r} (\tilde{z}_j')^2 = \|\mathbf{z}'\|^2 \leq \|\mathbf{x}'\|^2 \nu_1^2, \quad (74)$$

where ν_1 is the maximum singular value of the effective channel $\mathbf{W}_{\text{RF}}^* \mathbf{H} \mathbf{F}_{\text{RF}}$, we have

$$\mathcal{H}(\mathbf{r}|\mathbf{x} = \mathbf{x}') \geq 2N_{\text{RF}}^r \mathcal{H}_b \left(Q \left(\sqrt{\frac{\|\mathbf{x}'\|^2 \nu_1^2}{N_{\text{RF}}^r \sigma_{\text{N}}^2}} \right) \right) \quad (75)$$

by Jensen's inequality since $\mathcal{H}_b(Q(\sqrt{x}))$ is decreasing and convex in x (see [66] for the proof of convexity).

The conditional entropy of \mathbf{r} is,

$$\mathcal{H}(\mathbf{r}|\mathbf{x}) = \mathbb{E}_{\mathbf{x}} \left[2N_{\text{RF}}^r \mathcal{H}_b \left(Q \left(\sqrt{\frac{\|\mathbf{x}\|^2 \nu_1^2}{N_{\text{RF}}^r \sigma_{\text{N}}^2}} \right) \right) \right]. \quad (76)$$

Since $\mathcal{H}_b(Q(\sqrt{z}))$ is convex, then

$$\mathcal{H}(\mathbf{r}|\mathbf{x}) \geq 2N_{\text{RF}}^r \mathcal{H}_b \left(Q \left(\sqrt{\frac{\mathbb{E}[\|\mathbf{x}\|^2] \nu_1^2}{N_{\text{RF}}^r \sigma_{\text{N}}^2}} \right) \right). \quad (77)$$

We want to minimize $\mathcal{H}(\mathbf{r}|\mathbf{x})$ subject to the power constraint $\mathbb{E}[\|\mathbf{F}_{\text{RF}} \mathbf{x}\|^2] \leq P_t$, which is equivalent to $\mathbb{E}[\|\mathbf{x}\|^2] \leq P_t$ by the assumption $\mathbf{F}_{\text{RF}}^* \mathbf{F}_{\text{RF}} = \mathbf{I}$. As $\mathcal{H}_b(Q(\sqrt{z}))$ is decreasing in z , we have

$$\mathcal{H}(\mathbf{r}|\mathbf{x}) \geq 2N_{\text{RF}}^r \mathcal{H}_b \left(Q \left(\sqrt{\frac{\rho \nu_1^2}{N_{\text{RF}}^r}} \right) \right), \quad (78)$$

where $\rho \triangleq \frac{P_t}{\sigma_{\text{N}}^2}$. Therefore, the upper bound in (15) is obtained.

REFERENCES

- [1] J. Mo, A. Alkhateeb, S. Abu-Surra, and R. W. Heath Jr., "Achievable rates of hybrid architectures with few-bit ADC receivers," in *Proceedings of 20th International ITG Workshop on Smart Antennas*, March 2016, pp. 1–8.
- [2] T. Marzetta, "Noncooperative cellular wireless with unlimited numbers of base station antennas," *IEEE Transactions on Wireless Communications*, vol. 9, no. 11, pp. 3590–3600, November 2010.
- [3] F. Boccardi, R. Heath, A. Lozano, T. Marzetta, and P. Popovski, "Five disruptive technology directions for 5G," *IEEE Communications Magazine*, vol. 52, no. 2, pp. 74–80, Feb. 2014.
- [4] E. Larsson, O. Edfors, F. Tufvesson, and T. Marzetta, "Massive MIMO for next generation wireless systems," *IEEE Communications Magazine*, vol. 52, no. 2, pp. 186–195, Feb. 2014.
- [5] T. S. Rappaport, R. W. Heath Jr, R. C. Daniels, and J. N. Murdock, *Millimeter Wave Wireless Communications*. Pearson Education, 2014.
- [6] IEEE 802.11ad, "IEEE 802.11ad standard draft D0.1." [Online]. Available: www.ieee802.org/11/Reports/tgadupdate.htm
- [7] T. Rappaport, S. Sun, R. Mayzus, H. Zhao, Y. Azar, K. Wang, G. Wong, J. Schulz, M. Samimi, and F. Gutierrez, "Millimeter wave mobile communications for 5G cellular: It will work!" *IEEE Access*, vol. 1, pp. 335–349, May 2013.

- [8] W. Roh, J.-Y. Seol, J. Park, B. Lee, J. Lee, Y. Kim, J. Cho, K. Cheun, and F. Aryanfar, "Millimeter-wave beamforming as an enabling technology for 5G cellular communications: theoretical feasibility and prototype results," *IEEE Communications Magazine*, vol. 52, no. 2, pp. 106–113, February 2014.
- [9] A. Alkhateeb, J. Mo, N. Gonzalez-Prelcic, and R. Heath, "MIMO precoding and combining solutions for millimeter-wave systems," *IEEE Communications Magazine*, vol. 52, no. 12, pp. 122–131, Dec. 2014.
- [10] R. W. Heath Jr, N. Gonzalez-Prelcic, S. Rangan, W. Roh, and A. M. Sayeed, "An overview of signal processing techniques for millimeter wave MIMO systems," *IEEE J. Sel. Top. Signal Process.*, vol. 10, no. 3, pp. 436–453, 2016.
- [11] T. Bai and R. W. Heath, "Coverage and rate analysis for millimeter-wave cellular networks," *IEEE Trans. Wireless Commun.*, vol. 14, no. 2, pp. 1100–1114, Feb 2015.
- [12] B. Murmann, "ADC performance survey 1997-2016," 2016. [Online]. Available: <http://www.stanford.edu/~murmman/adcsurvey.html>
- [13] W. Hong, K.-H. Baek, Y. Lee, Y. Kim, and S.-T. Ko, "Study and prototyping of practically large-scale mmWave antenna systems for 5G cellular devices," *IEEE Commun. Mag.*, vol. 52, no. 9, pp. 63–69, September 2014.
- [14] A. Alkhateeb, J. Mo, N. Gonzalez-Prelcic, and R. W. Heath Jr, "MIMO precoding and combining solutions for millimeter-wave systems," *IEEE Commun. Mag.*, vol. 52, no. 12, pp. 122–131, December 2014.
- [15] O. El Ayach, S. Rajagopal, S. Abu-Surra, Z. Pi, and R. W. Heath Jr, "Spatially sparse precoding in millimeter wave MIMO systems," *IEEE Trans. Wireless Commun.*, vol. 13, no. 3, pp. 1499–1513, March 2014.
- [16] S. Han, C.-L. I, Z. Xu, and C. Rowell, "Large-scale antenna systems with hybrid analog and digital beamforming for millimeter wave 5G," *IEEE Communications Magazine*, vol. 53, no. 1, pp. 186–194, Jan. 2015.
- [17] J. Mo and R. W. Heath Jr., "Capacity analysis of one-bit quantized MIMO systems with transmitter channel state information," *IEEE Trans. Signal Processing*, vol. 63, no. 20, pp. 5498–5512, Oct 2015.
- [18] X. Zhang, A. Molisch, and S. Kung, "Variable-phase-shift-based RF-baseband codesign for MIMO antenna selection," *IEEE Transactions on Signal Processing*, vol. 53, no. 11, pp. 4091–4103, Nov. 2005.
- [19] V. Venkateswaran and A. van der Veen, "Analog beamforming in MIMO communications with phase shift networks and online channel estimation," *IEEE Transactions on Signal Processing*, vol. 58, no. 8, pp. 4131–4143, Aug. 2010.
- [20] A. Alkhateeb, O. El Ayach, G. Leus, and R. Heath, "Hybrid precoding for millimeter wave cellular systems with partial channel knowledge," in *Proc. of Information Theory and Applications Workshop (ITA)*, Feb 2013, pp. 1–5.
- [21] —, "Channel estimation and hybrid precoding for millimeter wave cellular systems," *IEEE Journal of Selected Topics in Signal Processing*, vol. 8, no. 5, pp. 831–846, Oct. 2014.
- [22] C. Rusu, R. Mndez-Rial, N. Gonzalez-Prelcicy, and R. W. Heath, "Low complexity hybrid sparse precoding and combining in millimeter wave mimo systems," in *Proceedings of the 2015 IEEE International Conference on Communications (ICC)*, June 2015, pp. 1340–1345.
- [23] C.-E. Chen, "An iterative hybrid transceiver design algorithm for millimeter wave MIMO systems," *IEEE Wireless Communications Letters*, vol. 4, no. 3, pp. 285–288, June 2015.
- [24] T. Bogale and L. B. Le, "Beamforming for multiuser massive MIMO systems: Digital versus hybrid analog-digital," in *IEEE Global Communications Conference (GLOBECOM)*, Dec. 2014, pp. 4066–4071.
- [25] F. Sohrabi and W. Yu, "Hybrid digital and analog beamforming design for large-scale MIMO systems," in *Proc. of the IEEE International Conf. on Acoustics, Speech and Signal Processing (ICASSP), Brisbane, Australia*, Apr. 2015.
- [26] L. Liang, W. Xu, and X. Dong, "Low-complexity hybrid precoding in massive multiuser MIMO systems," *IEEE Wireless Communications Letters*, vol. 3, no. 6, pp. 653–656, Dec 2014.
- [27] V. Venkateswaran and A.-J. van der Veen, "Analog beamforming in MIMO communications with phase shift networks and online channel estimation," *IEEE Trans. Signal Processing*, vol. 58, no. 8, pp. 4131–4143, 2010.
- [28] R. Walden, "Analog-to-digital converter survey and analysis," *IEEE J. Select. Areas Commun.*, vol. 17, no. 4, pp. 539–550, 1999.
- [29] B. Le, T. Rondeau, J. Reed, and C. Bostian, "Analog-to-digital converters," *IEEE Signal Processing Mag.*, vol. 22, no. 6, pp. 69–77, 2005.

- [30] A. Mezghani and J. Nosssek, "On ultra-wideband MIMO systems with 1-bit quantized outputs: Performance analysis and input optimization," in *Proceedings of IEEE International Symposium on Information Theory*, 2007, pp. 1286–1289.
- [31] A. Mezghani, M.-S. Khoufi, and J. A. Nosssek, "A modified MMSE receiver for quantized MIMO systems," *Proceedings of the ITG/IEEE WSA, Vienna, Austria*, 2007.
- [32] A. Mezghani and J. Nosssek, "Capacity lower bound of MIMO channels with output quantization and correlated noise," in *Proceedings of IEEE International Symposium on Information Theory*, 2012.
- [33] W. Zhang, "A general framework for transmission with transceiver distortion and some applications," *IEEE Trans. Commun.*, vol. 60, no. 2, pp. 384–399, February 2012.
- [34] J. Mo, P. Schniter, N. G. Prelcic, and R. W. Heath Jr., "Channel estimation in millimeter wave MIMO systems with one-bit quantization," in *Proceedings of the 2014 48th Asilomar Conference on Signals, Systems and Computers*, Nov 2014, pp. 957–961.
- [35] Q. Bai and J. Nosssek, "Energy efficiency maximization for 5G multi-antenna receivers," *Transactions on Emerging Telecommunications Technologies*, vol. 26, no. 1, pp. 3–14, 2015.
- [36] O. Orhan, E. Erkip, and S. Rangan, "Low Power Analog-to-Digital Conversion in Millimeter Wave Systems: Impact of Resolution and Bandwidth on Performance," in *Proc. of Information Theory and Applications (ITA) Workshop*, 2015.
- [37] S. Wang, Y. Li, and J. Wang, "Multiuser detection in massive spatial modulation MIMO with low-resolution ADCs," *IEEE Trans. Wireless Commun.*, vol. 14, no. 4, pp. 2156–2168, April 2015.
- [38] S. Jacobsson, G. Durisi, M. Coldrey, U. Gustavsson, and C. Studer, "One-bit massive MIMO: Channel estimation and high-order modulations," *arXiv preprint arXiv:1504.04540*, 2015.
- [39] J. Singh, O. Dabeer, and U. Madhow, "On the limits of communication with low-precision analog-to-digital conversion at the receiver," *IEEE Trans. Commun.*, vol. 57, no. 12, pp. 3629–3639, 2009.
- [40] J. Mo and R. W. Heath Jr., "High SNR capacity of millimeter wave MIMO systems with one-bit quantization," in *Proceedings of Information Theory and Applications Workshop (ITA), 2014*, Feb 2014, pp. 1–5.
- [41] J. Choi, J. Mo, and R. W. Heath Jr., "Near maximum-likelihood detector and channel estimator for uplink multiuser massive MIMO systems with one-bit ADCs," *IEEE Trans. Commun.*, vol. 64, no. 5, pp. 2005–2018, May 2016.
- [42] C. Mollen, J. Choi, E. G. Larsson, and R. W. H. Jr., "Performance of the wideband massive uplink MIMO with one-bit ADCs," *CoRR*, vol. abs/1602.07364, 2016. [Online]. Available: <http://arxiv.org/abs/1602.07364>
- [43] S. Jacobsson, G. Durisi, M. Coldrey, U. Gustavsson, and C. Studer, "Massive MIMO with low-resolution ADCs," *CoRR*, vol. abs/1602.01139, 2016. [Online]. Available: <http://arxiv.org/abs/1602.01139>
- [44] C. Studer and G. Durisi, "Quantized massive MU-MIMO-OFDM uplink," *IEEE Trans. Commun.*, vol. 64, no. 6, pp. 2387–2399, June 2016.
- [45] B. Murmann, "Energy limits in A/D converters," in *Faible Tension Faible Consommation (FTFC), 2013 IEEE*, June 2013, pp. 1–4.
- [46] H. Ghauch, T. Kim, M. Bengtsson, and M. Skoglund, "Subspace estimation and decomposition for large millimeter-wave mimo systems," *submitted to IEEE Journal of Selected Topics in Signal Processing*, *arXiv preprint arXiv:1507.00287*, 2015.
- [47] J. Mo, P. Schniter, and R. W. Heath Jr., "Channel estimation in broadband millimeter wave MIMO systems with few-bit ADCs," *arXiv preprint arXiv:1610.02735*, 2016.
- [48] U. Kamilov, V. Goyal, and S. Rangan, "Message-passing de-quantization with applications to compressed sensing," *IEEE Trans. Signal Processing*, vol. 60, no. 12, pp. 6270–6281, Dec 2012.
- [49] A. Molisch and X. Zhang, "FFT-based hybrid antenna selection schemes for spatially correlated MIMO channels," *IEEE Commun. Lett.*, vol. 8, no. 1, pp. 36–38, Jan 2004.
- [50] C. R. Rao, "Separation theorems for singular values of matrices and their applications in multivariate analysis," *Journal of Multivariate Analysis*, vol. 9, no. 3, pp. 362–377, 1979.
- [51] D. P. Palomar, J. M. Cioffi, and M. A. Lagunas, "Joint Tx-Rx beamforming design for multicarrier MIMO channels: a unified framework for convex optimization," *IEEE Trans. Signal Processing*, vol. 51, no. 9, pp. 2381–2401, Sept 2003.

- [52] J. A. Tropp, I. S. Dhillon, R. W. Heath, and T. Strohmer, "Designing structured tight frames via an alternating projection method," *IEEE Trans. Inform. Theory*, vol. 51, no. 1, pp. 188–209, 2005.
- [53] A. Sayeed, "Deconstructing multiantenna fading channels," *IEEE Trans. Signal Processing*, vol. 50, no. 10, pp. 2563–2579, Oct 2002.
- [54] T. M. Cover and J. A. Thomas, *Elements of information theory*. John Wiley & Sons, 2012.
- [55] J. G. Proakis, "Digital communications." *McGraw-Hill, New York*, 2008.
- [56] A. Fletcher, S. Rangan, V. Goyal, and K. Ramchandran, "Robust predictive quantization: Analysis and design via convex optimization," vol. 1, no. 4, pp. 618–632, Dec 2007.
- [57] J. Max, "Quantizing for minimum distortion," *IRE Transactions on Information Theory*, vol. 6, no. 1, pp. 7–12, 1960.
- [58] S. Lloyd, "Least squares quantization in PCM," *IEEE Trans. Inform. Theory*, vol. 28, no. 2, pp. 129–137, Mar 1982.
- [59] A. Gersho and R. M. Gray, *Vector quantization and signal compression*. Springer Science & Business Media, 2012, vol. 159.
- [60] M. Akdeniz, Y. Liu, M. Samimi, S. Sun, S. Rangan, T. Rappaport, and E. Erkip, "Millimeter wave channel modeling and cellular capacity evaluation," *IEEE J. Select. Areas Commun.*, vol. 32, no. 6, pp. 1164–1179, June 2014.
- [61] T. Rappaport, G. Maccartney, M. Samimi, and S. Sun, "Wideband millimeter-wave propagation measurements and channel models for future wireless communication system design," *IEEE Trans. Commun.*, vol. 63, no. 9, pp. 3029–3056, Sept 2015.
- [62] "5G channel model for bands up to 100 GHz," Tech. Rep., 2015.
- [63] R. Mndez-Rial, C. Rusu, N. Gonzalez-Prelcic, A. Alkhateeb, and R. W. H. Jr, "Hybrid MIMO architectures for millimeter wave communications: Phase shifters or switches?" *IEEE Access*, vol. 4, pp. 247–267, 2016.
- [64] Y.-H. Lin and H. Wang, "A low phase and gain error passive phase shifter in 90 nm CMOS for 60 GHz phase array system application," in *Proceedings of the 2016 IEEE MTT-S International Microwave Symposium (IMS)*, May 2016, pp. 1–4.
- [65] A. M. A. Ali, H. Dinc, P. Bhoraskar, C. Dillon, S. Puckett, B. Gray, C. Speir, J. Lanford, J. Brunsilus, P. R. Derounian, B. Jeffries, U. Mehta, M. McShea, and R. Stop, "A 14 Bit 1 GS/s RF Sampling Pipelined ADC With Background Calibration," *IEEE J. Solid-State Circuits*, vol. 49, no. 12, pp. 2857–2867, Dec 2014.
- [66] O. Dabeer, J. Singh, and U. Madhow, "On the limits of communication performance with one-bit analog-to-digital conversion," in *Proceedings of the IEEE 7th Workshop on Signal Processing Advances in Wireless Communications*, 2006, pp. 1–5.